The role of induced entrainment in past stratiform cloud seeding experiments

Article · December 2010

CITATIONS
0

READS
105

1 author:

Chris J. Walcek
University at Albany, The State University of New York
59 PUBLICATIONS **3,272** CITATIONS

SEE PROFILE

Title: The Role of Evaporation & Cloud-Top Entrainment Instability in Aircraft Seeding Experiments of Supercooled Stratus Clouds.

Author: Chris J. Walcek, State University of NY at Albany

Submitted 28 February 2013

Corresponding author address: ASRC-CESTM, 251Fuller Rd., Albany, NY 12203

email: cwalcek@albany.edu

Abstract- Cloud seeding experiments carried out during the 1940s showed unambiguously that aircraft flying immediately above supercooled stratiform clouds can induce dissipation tracks. The accepted explanation involves nucleation and growth of ice. Recent observations show cloud dissipation induced by commercial aircraft that are not dispensing seeding agents. Here an alternate explanation of aircraft-induced dissipation of stable clouds is proposed that does not involve ice formation. Aircraft flying above a cloud will force warm, dry air into a cloud. The resulting turbulent mixing can under many conditions trigger an unstable sequence of evaporation and downdrafts that can dissipate wide swaths of cloud via the mechanism of cloud top entrainment instability (CTEI). The dynamics of this mechanism are the reverse of the seeding process. Freezing heats a cloud, while evaporation of the same water mass produces cooling. The potential unstable impacts of aircraft turbulence and downwash-induced evaporation have been neglected or poorly accounted for in past explanations of stratiform cloud seeding from above. While ice formation can be occurring in seeded clouds, it is suggested here that evaporation effects can under many conditions dominate the dissipation process at the tops of supercooled clouds. Here the mechanism of aircraft downwash is reviewed, and CTEI is described. If significant evaporation occurs as aircraft fly close to the tops of stratiform clouds, then current and past textbooks describing cloud seeding provide only a partial explanation of the physics and dynamics of planned or inadvertent cloud seeding experiments involving stratiform clouds seeded from above.

1 1. Introduction

2 Schaefer (1946) showed that streams of homogeneously nucleated ice crystals ("diamond dust")
3 with radii less than ~25μm spontaneously form in the wake of dry ice fragments (T=-80˚C)
4 dropped through a laboratory freezer containing a supercooled cloud. In laboratory clouds, these
5 nuclei grew into planar hexagonal snow crystals with radii of 30-35 μm after about 4 minutes.

6 Following this discovery, crushed dry ice pellets were dropped from aircraft inducing spectacular
7 effects, and in 1947 "Project CIRRUS" was initiated to further investigate cloud seeding.
8 CIRRUS was a collaboration of General Electric, the US Army Signal Corps, the Office of
9 Naval Research, and the U. S. Air Force that was active from 1947 to 1952, and numerous cloud
10 types (stratiform, convective and even hurricanes) were seeded at locations throughout the U. S.
11 utilizing multiple aircraft on over 100 seeding and observation flights.

12 Of all the clouds seeded in project CIRRUS, the experiments showing the most dramatic results
13 were aircraft flying just above the tops of stratiform cloud layers dropping small (5-10mm
14 diameter) dry ice pellets into supercooled clouds. Under these conditions, 2-3 km wide swaths
15 under the flight path were dissipated within 30 minutes. Fig. 1 is an example of a famous figure
16 reproduced in numerous standard meteorology textbooks (e. g. Lutgens et al., 2006).

17 For over 50 years, the classical explanation for the dissipated cloud tracks shown in Fig. 1,
18 described in many meteorology textbooks (Mason, 1957; Miller and Anthes 1980; Wallace and
19 Hobbs 1977, 2006; Rogers and Yau 1989; Moran, 1994; Danielson et al. 2003; Aguado and Burt,
20 2009) is that homogeneously nucleated ice particles, formed in the wake of falling dry ice
21 pellets, induced rapid ice crystal growth converting supercooled liquid to ice. In a supercooled
22 liquid cloud, the water vapor pressure is approximately saturated with respect to liquid, and any

seeded ice particles will experience a significant supersaturation and thus grow rapidly via the Bergeron 3-phase process, while liquid drops evaporate. If there are much fewer numbers of ice particles than initial droplets, the crystals can grow large enough to fall out of the seeded region, or the cloud becomes optically thinner due to the same water mass being spread over fewer particles, leaving a dissipated cloud path below the seeding flight track.

Although it is not usually acknowledged in the above references of cloud seeding and dissipation, the wide lateral area affected by seeding is attributed to a dynamic feedback triggered by latent heat release during the freezing of supercooled liquid and subsequent ice condensation and growth producing positive buoyancy. Turbulence generated by the heated air mixes ice particles into neighboring ice-free regions, thus propagating the freezing-turbulence process laterally for distances 1-2 km perpendicular to the flight path.

More recently, Heymsfield et al., (2010) shows high-resolution MODIS satellite imagery (Fig. 2) of an approximately 240x240 km^2 area in central US covered by a supercooled stratiform cloud layer containing more than 20 "canal" tracks that were produced by commercial aircraft over Texas in Jan 2007. The clouds shown in Fig. 2 are identified by Heymsfield et al., (2011) to be at an altitude of 7.7 km at -30˚C and about 150m thick composed of supercooled liquid drops. Heymsfield et al. (2010, 2011) attributes the cloud dissipation tracks to the same mechanism described above, except the seeding is hypothesized to occur "inadvertently" at the tips of propeller blades or over the wings, where transitory air expansion can produce minute regions where temperatures are cooled, inducing ice nucleation.

All previous analyses of supercooled cloud seeding have ignored or greatly underestimated the effects of aircraft downwash. There is no mention of aircraft wake effects at all in the CIRRUS

project reports and publications, even though the senior project scientists involved were familiar with downwash cloud effects (Langmuir and Forbes, 1936). More recent cloud seeding experiments (Rosenfeld et al. 2005; Yu et al., 2005) mention nothing about possible evaporation effects associated with wake downwash. Heymsfield et al. (2010) acknowledge that aircraft wake dynamics can play a role in observed cloud dissipation, and considers evaporation resulting only from adiabatic warming due to downward displacement of cloudy wake air. They dismiss the evaporated areas as being too narrow, and suggest that evaporation cannot be very important. However, Heymsfield et al., (2010) does not consider evaporation associated with mixing of cloud-free air into the cloud from above.

Heymsfield et al., (2011) perform a 50m-resolution (cloud vertically resolved by three layers) computational simulation of the effects of introducing a large number of ice crystals over a relatively large area (250m, seven times the Boeing 737 wingspan of 36m) and finds that a small precipitation ice-forming region forms near the middle of the seeded region, but the hole growth is driven by subsequent evaporation of the cloud generated by turbulence at the edge of the holes. Heymsfield et al.'s simulation did not include turbulence or downdraft of the initial wake downwash, but clearly showed the importance of evaporation effects in producing holes in clouds near aircraft. Here we suggest that aircraft downwash, displacing large amounts of dry air from above cloud top into the cloud would trigger the evaporation cycle simulated by Heymsfield et al. (2011).

Mixing cloud-free air into a cloud will evaporate cloudwater. Evaporation of cloudwater near the tops of stable stratiform clouds can produce COLD, negatively buoyant air that has the potential to release considerable Cloud Top Entrainment Instability (CTEI) as described in Yamagichi and Randall (2008). The energy released by evaporation can cool air by amounts comparable to or

greater than the heating associated with freezing the same amount of water, providing an ample energy reservoir for a positive-feedback dynamics/evaporation mechanism that mixes dry air near cloud top into the cooler cloudy layer. Past studies have shown that CTEI effects can be limited since little turbulence exists near the tops of stable stratiform clouds to trigger the release of available CTEI energy. Aircraft-induced turbulence and downwash provide precisely the triggering mechanism necessary to release CTEI near stable stratiform cloud tops, as long as the gradients of relative humidity and temperature satisfy accepted CTEI criterion.

During the preparation of this paper, numerous archived sponsor reports from project CIRRUS, photographs, and flight notes and information from the Vincent Schaefer archives at the University at Albany Library were analyzed, and previously unpublished observations pertinent to this paper are presented here.

In the next sections, aircraft wake downwash and turbulence is described and quantified. Following this, the dynamics and microphysics of CTEI is summarized. The dynamics of the propagation mechanism associated with freezing/heating and evaporation/cooling are then described and compared. Another section discusses numerous observations of past cloud seeding studies, showing how CTEI can explain many observed cloud seeding effects within supercooled stratiform clouds. Finally, there is a section devoted to suggestions for future seeding experiments that would shed light on the neglected role that CTEI might play in modifying cloud properties.

2. Aircraft downwash & turbulence

During flight, aircraft generate a wake of considerable turbulence due to aerodynamic drag, and also produce a net downward displacement of air ("wake downwash") in order to generate lift

1 opposing gravity. This downwash induces a pair of horizontal vortices that descend through
2 stagnant air, dissipating below and aft of the aircraft within a few minutes. Fig. 3 shows a picture
3 of a descending vortex pair below a commercial Boeing 777-200 as it approached London
4 Gatwick airport at 7AM local time in July 2006.

5 Aircraft wings produce upward lift by accelerating air over the tops of the wings relative to the
6 air flowing under the wings. Air is then diverted down under and aft of the wings. Newton's
7 third law dictates that while flying, the aircraft weight is balanced by an upward lift force
8 generated by the wings. For propeller-driven aircraft, some of the air pushed back by the blades
9 (producing forward thrust) can contribute to lift if it is directed slightly downward. The "equal
10 and opposite" lift force consists of a flux of air accelerated down below the airframe and wings.

11 $$m_{air}\frac{dw}{dt} = \frac{dm_{air}}{dt}w = m_{plane}g \ . \qquad (1)$$

12 Here m_{air} is the mass of air pushed down (kg), w is the impulse downward vertical velocity
13 induced by the wings immediately below and behind the wings (m s^{-1}), m_{plane} is the aircraft mass
14 (kg), and g is the gravitational acceleration. The mass flux of air pushed down per unit time
15 (dm_{air}/dt, kg_{air} s^{-1}) is the product of the air density (ϱ_{air}), the accelerated vertical velocity
16 perturbation, and the horizontal area below the wings/airframe (A_{wing}) being pushed down.

17 $$\frac{dm_{air}}{dt} = A_{wing}\rho_{air}w \ . \qquad (2)$$

18 Substituting (2) into (1), the force balance is expressed as

19 $$m_{\text{plane}}\ \text{g} = A_{\text{wing}}\ \varrho_{\text{air}}\ w^2 \ . \qquad (3)$$

20 Solving for w

$$w = \sqrt{\frac{m_{plane} g}{A_{wing} \rho_{air}}} \quad , \tag{4}$$

The wing area of the B-17 aircraft used during the project CIRRUS seeding experiments is 132 m^2, and the empty mass is 16400 kg. Using an air density at flight altitudes (1 kg m^{-3}) yields downward velocities immediately below the seeding aircraft of 35 m s^{-1}.

As the downward-moving rotating cylinders of wake vortex air descend through stagnant air, local shear-induced turbulent mixing will cause drag and turbulent entrainment that slows and ultimately stops the downward propagation. Classical parcel theory suggests that the characteristic (e-folding) length scale for frictional drag to halt the vertical motion of a spherical "bubble" of air is on the order of the horizontal size of the downward-moving parcel, which is approximately the aircraft wingspan. However, this displacement length scale can be several factors longer for a 2-D descending "cylinder" due to the fact that a 2-D cylinder-shaped parcel has much less surface area over which drag and entrainment acts per unit volume relative to a spherical parcel. In addition, the relatively stable dynamics of a tornado-like vortex can further enhance the lifetime of the descending vortex pair. Therefore one would expect that downward motions below an aircraft might propagate several wingspans below an aircraft, which for the B17 used in project CIRRUS cloud seeding experiments is 32 m.

Using a semi-empirical model evaluated with test flight observations, Greene (1986) shows that atmospheric stability strongly affects the downward air displacement beneath an aircraft, and downward displacements of 2-8 wingspans can occur before the descending vortices decay. Fig. 4 is derived from Greene (1986) showing the calculated depth to which wake vortices descend before dissipation. Greene's calculations are general, with atmospheric stability and

displacements normalized to wingspan and initial downwash velocity. Here his nondimensional numbers have been converted to conventional stabilities and distances using the properties of the B17 seeding aircraft used during project CIRRUS. Fig. 4 shows that for the conditions of several clouds seeded during project CIRRUS, downwash below the seeding aircraft probably extended 150-200m below the flight level, well into the cloudy layer. These approximate calculations are consistent with Heymsfield et al., (2010), who estimates that wake downwash can penetrate 150-400 meters below an aircraft.

In addition to producing a lift-induced downwash, aircraft must overcome considerable aerodynamic ("parasitic") drag that is proportional to the cube of aircraft speed. At flight speeds, most aircraft power is devoted to overcoming aerodynamic drag that dominates over lifting power requirements. Thus there is a large amount of turbulent kinetic energy initially contained in eddies that have sizes proportional to the aircraft frontal dimensions (3-10m), with eddy velocity scales comparable to the flight speeds (~70 m s^{-1}). Therefore, turbulent diffusion coefficients (K) should be in the range of 200-700 m^2 s^{-1} immediately behind an aircraft, which is comparable to the amount of turbulence in the middle of a well-developed afternoon convective boundary layer. In a stable environment this turbulence will quickly dissipate within a few minutes, but during dissipation the turbulent kinetic energy will propagate laterally over a distance considerably larger than the aircraft dimensions. A rough scaling suggests that the vertical depth influenced by the turbulence could be in the range

$$\Delta z_{mix} = \sqrt{2Kt} \ , \qquad (5)$$

where t is the dissipation time scale (~5 min, 300s?), and K would be about half the values estimated above since K is decreasing to zero during the time interval. Using an average K of 100

$m^2\ s^{-1}$ acting over 300s (5 minutes), Δz_{mix} = 200m. At the base of this "induced mixing region", air would be adiabatically heated while it was forced down a distance Δz_{mix} from above. This extremely crude estimate suggests that it might be possible to dynamically "feel" the presence of an aircraft if one were within 200m of the plane flying past at 70 $m\ s^{-1}$, which is not an unreasonable scaling estimate.

Both the turbulence and downwash induced by aircraft have the potential to move air vertically from heights approximately 100-200m above cloud top into a cloud, and for the measured static stabilities of several project CIRRUS seeding experiments ($\partial\theta/\partial z \sim +6$°C/km), air mixed into a cloud would be 0.1 - 1.2 °C warmer than the cloud, depending on how high the aircraft flew above cloud top and the ambient stability of the air above the cloud.

3. Cloud Top Entrainment Instability

Lilly (1968) proposed that statically stable clouds could be potentially unstable if there were a negative gradient of equivalent potential temperature in a cloudy environment. Under certain conditions, warm dry air mixed into a cloud can produce sufficient evaporation to make mixtures colder than the unmixed cloudy air, thus generating negative buoyancy. Under these conditions there is a potential for a positive feedback between mixing creating negatively buoyant air, which induces more mixing propagating the process. Yamaguchi and Randall (2008) describe the history and physics of this cloud top entrainment instability (CTEI) mechanism. This instability will not always be released if there is no triggering mechanism. Usually the tops of supercooled stratiform clouds exist in statically stable environments with relatively little ambient turbulence, and there is no triggering mechanism. Aircraft-induced turbulence and wake vortices below an aircraft can provide precisely the trigger necessary to release CTEI.

Once aircraft-induced turbulence and its wake vortex penetrate into a stable stratiform cloud top, the stagnant cloudy air will mix with dry hotter air that has been displaced downward and adiabatically heated. Some evaporation will occur as cloudy and clear air mix, and beyond some critical mixing fraction of outside air, cloudwater will totally evaporate. Fig. 5 shows schematically the temperature structure and the vertical motions that theoretically can result from the induced mixing of above-cloud air into a cloud.

Fig. 6 shows the liquid water virtual temperature difference [$T_v = T(1-q_l)/(1-0.608q_v)$] between mixtures of cloudy and clear air relative to the unmixed surrounding cloud as a function of the mixing fraction (f_{cld}) of cloudy air in the mixture. This temperature difference is calculated assuming that any evaporating liquid induced by the mixing cools the mixture until it reaches saturation, or until all liquid evaporates. The total water content of a mixture of cloudy and clear air is the fractionally weighted total water content of the two components of the mixture. For the cloud portion, this consists of vapor (q_{vcld}) and liquid (q_{lcld}), but only vapor (q_{ve}) in the cloud-free air entrained into the cloud.

$$Q_{tot} = (q_{lcld} + q_{vcld})f_{cld} + q_{ve}(1-f_{cld}) \ , \tag{6}$$

The water vapor content of the unmixed cloudy air will be saturated at the specified cloud temperature [$q_{vcld} = q_{sat}(T_{cld})$]. The water vapor content of the environmental air mixed into the cloud is determined by its relative humidity [$q_{ve} = Rh_e \, q_{sat}(T_{env})$].

An initial estimate of the temperature (T_i) and liquid water mixing ratio (q_{li}) of a mixture of cloudy and clear air can be obtained by linearly weighting the mixing fraction

$$q_{li} = q_{lcld} f_{cld} \ . \tag{7}$$

$$T_i = T_{cld} f_{cld} + T_{env}(1-f_{cld}) \; . \tag{8}$$

This "initial estimate" will generally not be saturated. As cloudy and clear air mix, small cloud drops will quickly evaporate if the initial mixture is below 100% Rh. Evaporation reduces the liquid water content and simultaneously cools the temperature due latent heat of evaporation. The vapor mixing ratio in the final mixture will be either the total water content of the mixture (if all liquid evaporates), or it will be saturated at the equilibrium mixture temperature

$$q_{vmix} = \min[Q_{tot} \; , q_{sat}(T_{mix}) \;]. \tag{9}$$

The liquid water content of the mixture is any remaining water that does not evaporate

$$q_{lmix} = Q_{tot} - q_{vmix}. \tag{10}$$

Water that evaporates during the mixing process cools the parcel according to

$$c_p(T_{fi} - T_{mix}) = L_e \, (q_{li} - q_{lmix}) \; , \tag{11}$$

Where c_p is the heat capacity of air (1004 J $^{\circ}C^{-1}$ kg^{-1}), and L_e is the latent heat of liquid evaporation (2.5×10^6 J kg^{-1}).

Equations (6-11) represent an implicit relationship of the final mixture temperature (T_{mix}), requiring iterative solution due to the exponential relationship between saturation vapor mixing ratio and temperature.

Fig. 6 shows that if 95% Rh dry parcels are mixed into a cloud, none of the mixtures with the surrounding cloud will be negatively buoyant. In contrast, at relative humidity of 50 or 70%, well over half of the possible mixing fractions are negatively buoyant. The coldest negatively buoyant mixtures are produced at precisely the mixing point where all cloudwater in the mixture

evaporates, leaving the mixture at 100% Rh. The maximum cooling that can be produced is comparable in magnitude to the positive stable temperature difference between the unmixed dry parcel and cloud. Without mixing (f_{cld}=0), dry parcels pushed down into a cloud by aircraft downwash will experience a strong upward-directed restoring buoyancy force. However, with mixing and evaporation, a downward acceleration can be produced, amplifying the initial downward impulse of air into the cloud. Under these conditions, it would be possible to trigger a positive feedback process whereby evaporation induces cooling, which generates more downward-directed air that mixes and evaporates cloudwater, propagating the cycle of cloud-top entrainment instability.

Fig. 6 shows buoyancy calculations for only one temperature difference. Fig. 7 shows the maximum negative temperature difference (Fig. 7a) and the fraction of mixtures that are negatively buoyant (Fig. 7b) over a wide range of ΔT and environmental Rh. For air that is adiabatically displaced into a cloud from above, this temperature difference will be proportional to the downwash vertical displacement (Δz) multiplied by the difference between the environmental lapse rate above the cloud and the dry adiabatic lapse rate [$\Delta T = \Delta z\ (\partial T/\partial z + g/c_p)$], shown schematically in Fig. 5. Therefore the horizontal axes of Fig 7 will be proportional to either the static stability ($\partial\theta/\partial z$) or the height at which an aircraft flies above cloud top. When warmer air is pushed into a cloud, there is no potential for unstable motions if no evaporation occurs. The grey area on Fig. 7 delineates the regime of warmer temperature differences and Rh that can produce unstable motions in an otherwise stable environment as a result of evaporative cooling. There are wide ranges of conditions that have the potential for generating negative buoyancy.

Fig. 7 summarizes the CTEI instability criterion, and shows the temperature and humidity regimes where the intensity and/or likelihood of CTEI effects should occur near the tops of clouds. The likelihood of CTEI decreases as hotter air is pushed into a cloud. Negatively buoyant unstable conditions occur below a threshold relative humidity, and as the temperature difference (ΔT) of dry air pushed into a cloud increases, this Rh threshold decreases. For a 1 ˚C temperature difference, which for the conditions shown on Fig. 5 corresponding to a adiabatic displacement of about 170m (if the measured $\partial T/\partial z$ in the cloud -4˚C/km extends above cloud top), the Rh of the dry air pushed into the cloud must be below about 80% in order to generate negatively buoyant mixtures and trigger cloud top instabilities.

4. Thermodynamics of the positive-feedback propagation mechanism

It is well recognized that in order to explain the relatively wide areas affected by seeding along a narrow track, a dynamic positive feedback mechanism that propagates the microphysical disturbance must occur. Fig. 8 shows schematically the thermodynamics of the hypothesized propagation mechanism that can occur during cloud seeding. It is assumed that a turbulent mechanism driven by latent heat released during freezing is responsible for generating positively buoyant parcels, generating turbulence that mixes ice nuclei into the neighboring ice-free cloud, thus propagating the cycle of freezing, heating and turbulence. The latent heat responsible for generating turbulence results not only from converting supercooled liquid to ice, but also from the condensation of vapor to ice in the initially water-saturated cloud, bringing the cloud to a lower ice-saturated vapor pressure.

The potential heating associated with freezing supercooled cloudwater will be proportional to the amount of liquid frozen and the vapor in excess of ice saturation in the cloud:

$$T_{heat} - T_{cld} = \frac{L_f}{c_p} q_l + \frac{L_s}{c_p}\left(q_{sl}(T_{cld}) - q_{si}(T_{heat})\right) \ , \qquad (12)$$

where L_f and L_s are the latent heat of liquid freezing (3.21×10^5 J kg^{-1} at -6°C) and sublimation (2.84×10^6 J kg^{-1}), c_p is the heat capacity of air (1004 J °K), q_l is the liquid water content (g kg^{-1}), $q_{sl}(T_{cld})$ is the initial vapor mixing ratio in the cloud, assumed saturated with respect to liquid at the cloud temperature, and $q_{si}(T_{heat})$ is the final water vapor mixing ratio in the frozen cloud, saturated with respect to ice at a slightly warmer temperature. The warming must be calculated iteratively since the q_{si} is exponentially related to the warmer temperature. Fig. 9a shows this heating as a function of temperature below freezing at different pressure levels in the atmosphere for a cloud of q_l= 0.2 g kg^{-1} liquid water. The lower heating curve shown in Fig. 9a shows the contribution of the warming due to liquid freezing only, showing that the freezing of liquid contributes only a small fraction to the potential warming. The maximum heating occurs at -18 to -14 °C, and except for temperatures very close to freezing, a vast majority of the heating is due to direct vapor deposition into ice and therefore the heating is proportional to the vapor pressure difference between ice and liquid, and relatively insensitive to cloud liquid water content. This suggests that clouds are not even necessary for seeding to accomplish these effects, and supercooled clouds only tell where the atmosphere is likely liquid saturated.

Fig. 9b shows the potential cooling that can occur as warm, dry air mixes into a supercooled cloud evaporating all initial liquid. The potential cooling ΔT_{cool} following evaporation will be given by

$$T_{cld} - T_{cool} = (f-1)(T_{env} - T_{cld}) + f\frac{L_e}{c_p} q_l \ . \qquad (13)$$

Here L_e is the latent heat of evaporation (2.5×10^6 J kg^{-1}), T_{env} is the temperature of the warmer environmental air pushed into the cooler cloud (T_{cld}), and f is the fraction of cloudy air in a mixture of clear and cloudy air that just evaporates all cloudwater, resulting in a mixture that is saturated. As noted in Fig. 6, not all mixtures of cloudy and clear air produce air colder than the surrounding cloud, and the first term involving T_{env} on the right hand side of Eq. 13 is negative (warmer than surrounding cloud) since f <1, and all cooling results from the q_l term evaporating condensed water. The final water content in a mixture of clear and cloudy air is constrained by the following water-balance relation

$$q_{sat}(T_{cool}) = f\left[q_l + q_{sat}(T_{cld})\right] + (1-f)Rh_e q_{sat}(T_{env}) \ . \qquad (14)$$

Eqs. 13-14 must be solved iteratively. Fig. 9b shows that the potential cooling grows monotonically with increasing temperature, and is approximately linearly proportional to water content of the cloud, which contrasts with the warming due to freezing which only slightly changes as cloud water content increases.

Fig. 9a shows that in the region around individual falling dry ice pellets, seeding can produce regions that are several tenths of a ˚C warmer than the surrounding unfrozen cloud. In contrast, Fig. 9b shows that along some mixing regions of an aircraft-induced downwash pushed into a cloud, evaporation can potentially produce mixtures several tenths ˚C colder than the surrounding cloud.

During cloud seeding, both freezing-induced heating and evaporation-induced cooling could be simultaneously occurring as seeding aircraft fly just above the tops of supercooled clouds. However, these heated and cooled areas will initially be segregated. The vortex-induced evaporation area will wrap around the descending vortex and initially be restricted to a finite

volume of air at the interface of the cloudy and clear air along the edges of the downwash vortex. The evaporation region will extend horizontally perpendicular to the flight path over the initial horizontal scale of the wingspan-wide wake downwash. In contrast, heating induced by freezing will be restricted to cylindrical regions around each falling dry ice pellet, extending well below the wake downwash along a line directly under the flight track. These two locally hot and cold regions could interact as their potentially unstable mechanisms propagate laterally away from the initial disturbance.

Both cooling associated with evaporation and mixing, and heating associated with ice formation can be considered together, and Fig. 10 shows the calculated distribution of heating/cooling that potentially can occur considering both of these effects. Here it is assumed that all liquid freezes during the mixing/evaporation process, and the final mixture equilibrates saturated with respect to ice rather than liquid. This figure shows that seeding and ice formation will generate positive buoyancy in cloudy air that does not experience much mixing with cloud-free aircraft wake air. Any ice formed will evaporate as efficiently as liquid water due to mixing with warmer air, and the maximum cooling is only slightly reduced by the heating contributed by the freezing process. Therefore, even if there is ice production in seeded clouds, there is still considerable evaporative cooling effects related to CTEI as condensed liquid water or ice evaporates while mixing with wake downwash air near cloud top.

5. Discussion

These calculations demonstrate that microphysical effects of turbulent mixing of dry air forced into a cloud by aircraft downwash can be significant. The evaporative cooling and release of cloud top entrainment instability under the appropriate conditions could play a major role in the

observed dissipation of clouds that are influenced by aircraft flying near them. One prediction of this hypothesis is that this mechanism should occur whenever aircraft fly within a few 100m above cloud top and CTEI instability criterion are satisfied across the cloud top interface. The numerous aircraft-induced cloud effects shown in Fig. 2 are consistent with this hypothesis of CTEI-induced effects. In order to assess the potential for CTEI, it is necessary to perform relatively high vertical resolution measurements of the temperature, humidity, and cloudwater content throughout the depth of the downwash-influenced region below a flying aircraft. Such measurements have not been reported in past cloud seeding experiments.

Heymsfield et al., (2010)'s explanation of aircraft-induced cloud dissipation implies that only propeller aircraft flying WITHIN a cloud would induce cloud dissipation. The explanation proposed here works best for ALL aircraft flying above but very close to cloud top, as long as CTEI criteria are satisfied. Therefore another test of the validity of this mechanism would be to ascertain whether jet-powered aircraft flying above clouds produces tracks. If aircraft that are not actively seeding can produce these dissipated cloud tracks while flying slightly above cloud top, then the mechanism is likely CTEI-triggered.

In project CIRRUS sponsor reports, there were scattered observations of ice formation, and several visual reports suggesting no evidence of ice in dissipated cloud regions. While project CIRRUS did not routinely monitor conditions under seeding tracks, there were occasional observations from above which showed reflections from sunlight off the seeded paths that are characteristic of sunlight glinting from ice crystals (Schaefer 1950a). When no ice was observed, it was assumed to have fallen away from dissipated clouds as snow/precipitation from the seeded regions. An alternate explanation of no observed ice would be that evaporation was the primary mechanism dissipating the clouds beneath seeding tracks. It is not necessary for ice to fall from a

dissipated cloud for it to appear optically thinner than the surrounding cloud. The number of condensed particles can be reduced by 1-2 orders of magnitude during glaciation. If a supercooled cloud containing several hundred drops per cubic centimeter is converted to an ice cloud containing 1/10th to 1/100th that number density, the cloud would appear much "thinner" and even appear to have dissipated whether or not the larger ice particles fell from the cloud. Ice nucleation could be occurring during aircraft seeding operations, but it is suggested here that effects associated with ice formation would be superimposed and possibly even overwhelmed by evaporation effects associated with CTEI.

During one project CIRRUS seeding experiment (flight #83 on 18 Apr 1949, a figure "4" seeding pattern), there was an attempt to determine whether silver iodide (AgI) was as effective as dry ice in seeding clouds. Dry ice was dispensed along most of a 75-mile flight track, but during a one-mile stretch in the middle of the seeding pattern, small burning charcoal embers that were impregnated with an AgI solution were dropped instead of dry ice. During the time it took to switch the dispensing apparatus, approximately one mile on either side of the AgI seeding portion of the pattern, no seeding agents were dispensed from the aircraft. An observation aircraft flying higher than the seeding aircraft reported "no difference between the dry ice and AgI seeded" stretches of the seeding path, which at the time lent credence to the efficacy of AgI as a seeding agent. However, there was no mention in CIRRUS reports of the nonseeded portions of the flight track. Fig. 11 shows a photograph of the flight #83 "four" pattern, and the flight track on the right should contain two 1-mile stretches where no seeding agents were dispensed, encompassing both sides of a 1-mile stretch where burning charcoal-impregnated AgI was dispensed. While there is some evidence of unexplained "jogs" in the dissipation pattern (which are probably related to changing horizontal winds at cloud top), it is not clear that there are any

striking microphysical differences along two 1-mile portions on the right where no seeding agents were dispensed. However, it is possible that this photograph was taken after too much time had elapsed, and the "fore and aft" edges of the nonseeded portions of the flight track had merged, overcoming the nonseeded portions. Here it is suggested that evaporation effects overwhelmed any seeding effects, and Fig. 11 shows a cloudy track that has been evaporated due to CTEI triggered by the aircraft downwash, and thus no different effects were observed along two 1-mile stretches were no seeding agents were dispensed.

Another factor suggesting that seeding effects could be much smaller than CTEI effects relates to the differences in the cloud volume initially impacted by either the seeding agents or the downwash turbulence. During project CIRRUS seeding experiments, the dry ice was crushed into pellets with a diameter of about 1 cm. The pellets were dispensed through a small hole in the floor of the seeding aircraft at rates of less than 1-2 lbs per mile (280-560 g km^{-1}). The horizontal linear distance between individual dry ice pellets as they fell through the cloud deck can be calculated as

$$spacing = \frac{4\pi r^3 \rho_s}{3s} \quad , \tag{15}$$

where s is the seeding rate in g m^{-1}, ϱ_s is the seeding particle (dry ice) density (1.5 g cm^{-3}) and r is the dry ice pellet radius (=0.5 cm). Schaefer (1950b) reports that for seeding flight #83 (Fig. 10), dry ice was dispensed at a rate of ½ pound per mile (0.14 g m^{-1}). Therefore spacing between each descending dry ice pellet was about 5.6 meters. Any individual falling dry ice pellet will initially only influence an area of 1-2 meters at most around its fall path (~1-4 m^2, viewed from above). In contrast, the wake downwash area experiencing evaporation will span the entire vortex width, approximately the aircraft wingspan. Therefore, around each falling dry ice pellet, the wake

vortex evaporation area will be the product of the downwash width (32 m) and the pellet spacing (5.6m) = 179 m^2, an area 10-100 times greater than the seeded area. Clearly, downwash effects will dominate the initial impacted area if the downwash wake penetrates into the top of a cloud while the seeding aircraft flies above cloud top.

Fig. 12 shows more evidence of the importance of downwash effects. This picture was taken from an observation aircraft flying parallel to and several thousand feet above the seeding aircraft during CIRRUS flight #83 on 18 Apr 1949, a photograph of a portion of the same "figure-4" shown in Fig. 11 taken immediately following seeding during the initial formation of the dissipated cloud region. Using the B17 wingspan as a scale, in conjunction with the reported 99 m s^{-1} flight speed, one can construct an approximate time and length scale aft of the seeding aircraft, which is overlaid on the figure. It is obvious that visible cloud impacts are evident 4 seconds after flyover, which is barely time for the free-falling dry ice pellets to reach the cloud top. This 4 second time period is also considerably smaller than the time for any microphysical effects to occur. However, this 4 second time period coincides nicely with the time it takes a 30-40 m s^{-1} downdraft to reach cloud top. Even if dry ice pellets were carried by downwash, reaching the cloud top faster than free-fall time, Schaefer (1949) notes that in laboratory clouds, only 1-2 cm around seeded ice crystals are cleared of cloud drops in "a few seconds" as cloud drops evaporate and recondense on seeded crystals. Schaefer (1946) notes that it took 3-4 minutes for seeded ice crystals to grow to 35 μm, which was not enough time to totally glaciate a large cloudy area. This 3-4 minute time to grow a relatively small ice crystal in a supercooled cloud would put the snow crystal formation distance approximately 14 km behind the seeding aircraft, while Fig. 12 clearly shows a dissipated cloud track appearing within 0.5 km. Clearly

1 the growing wake region shown in Fig. 12 results primarily from a downwash penetrating into
2 the top layers of the cloud.

3 Furthermore, the wake region is shown to be growing in Fig. 12. The "canal" region grows from
4 about 1-2 wingspan to ~4 wingspans in width within about 15-20 seconds. This growth rate, if
5 allowed to continue, would easily produce the observed 1-2 mile wide dissipated paths within
6 20-30 minutes. Therefore it appears that the initial growth rate, which must be dominated by
7 wake downwash effects, could persist for the entire time during the 20-30 minute dissipation
8 process and subsequently produce the observed 1-2 km dissipation swath shown in Fig. 11.

9 It is possible, as suggested by Heymsfield et al (2010), that the preliminary wake effects shown
10 in Fig. 12 remain spatially confined and/or quickly dissipate, and microphysical effects could
11 then "take over" the subsequent dynamical propagation of the observed cloud dissipation. Any
12 heat released by ice formation would initially occur immediately along a "curtain" or line
13 penetrating well into the cloud right at the center of the wake downwash region. For the rest of
14 the wingspan-wide region at the interface of the wake downwash and cloud, evaporative cooling
15 effects could occur. It is possible that there are complex dynamic interactions between cooling
16 and evaporation in some regions of the perturbed cloud, and heating in the unevaporated cloud
17 regions influenced by seeding. Confirming whether any of these heating or cooling interactions
18 are occurring would require extremely high-resolution measurements and modeling tools capable
19 of resolving portions of turbulent eddy scales, on the order of 1-10 m.

20 Another observation in support of this evaporation mechanism of cloud dissipation is evident in
21 Figs. 1 and 11. Note that the cloud is only dissipated over a finite depth. According to the
22 freezing-seeding explanation, ice formation within a supercooled cloud should unstably

propagate wherever ice forms and falls. The dry ice pellets themselves should fall a considerable vertical distance into the cloud before subliminating. If precipitation-sized ice particles were produced, they should induce phase change throughout their descending path and clear the cloud all the way to the freezing level or through to cloud base if the entire cloud is below freezing. For the "racetrack" and "figure-4" clouds shown in Figs. 1 and 11, the entire cloud depth (0.7, 1.9 km) was below freezing, and yet dissipation only occurs in a restricted region near cloud top. As shown schematically on Fig. 5, cloud top entrainment instability will only influence a finite depth of the cloud layer near cloud top, given by

$$\Delta z_{CTEI} = \frac{\Delta T_{cool}}{\left(\frac{\partial T}{\partial z} - \frac{g}{c_p} \right)} \quad , \tag{16}$$

where ΔT_{cool} is the maximum amount of cooling produced by the CTEI process (shown in Figs. 7a, 9b and 10), $\partial T/\partial z$ is the temperature lapse rate below cloud top, g/c_p is the dry adiabatic lapse rate, the rate at which any CTEI-induced cooled parcels would heat during descent. Using the reported -4 ˚C/km lapse rate and $\Delta T_{cool} = 0.35$ ˚C (taken from a typical region of Fig. 7a), this produces a depth of about 60 meters cleared, which is a dissipation depth consistent with the cleared layer shown in Figs. 1 and 11.

It is possible that both evaporation and freezing effects could be occurring simultaneously within clouds that are overflown by seeding aircraft. An alternate way of interpreting past cloud seeding experiments is to suggest that aircraft "seed" a cloud with both turbulence and microphysical phase-change-inducing agents. If both effects are occurring, the explanation of what is happening along a dissipating cloud track becomes considerably more complex than the explanations offered in textbooks describing aircraft seeding.

Suggestions for future seeding experiments

For future cloud seeding investigations, an experimental protocol that would ascertain the importance of seeding-freezing relative to mixing-evaporation would be to simply stop the seeding for specified portions of the flight track and ascertain the differences between the seeded and unseeded portions of the flight track.

For dry ice seeding, a single dry ice particle could be dropped into a supercooled cloud from a high enough distance above cloud top to ensure that no downwash affects the cloud layer. According to the seeding-freezing mechanism, a 1-2 mile wide hole should develop. In project CIRRUS notes and reports, there were records of "single point" dry ice seeding drops with ambiguous results. Some "point drops" developed holes, while other drops showed negligible effects in stable cloud decks. The only way individual dissipation holes could occur with the CTEI mechanism would be for the aircraft to have momentarily descended to barely touch the cloud top right at the point of the single dry ice pellet drop, then immediately ascend to a higher flight elevation where the downwash would not penetrate to cloud top. There were no records of high-time-resolution flight altitude measurements during these CIRRUS "point drop" experiments, but this could be investigated in future cloud seeding experiments.

Another important measurement that would unambiguously ascertain whether CTEI evaporation effects are occurring would be to measure temperatures within and across the dissipated seeded track with a high time/space-resolution probe. According to the seeding/freezing dissipation mechanism, only air *warmer* than the surrounding cloud should be measured in the dissipated cloud region. In contrast, according to the downwash mixing/evaporation mechanism proposed

here, regions that are *colder* than the surrounding cloud should be measured at some points in the dissipated/evaporated cloud area if CTEI critera are satisfied.

If both mixing-induced evaporation and freezing are occurring in a downwash wake below a seeding aircraft, Fig. 10 shows that partially evaporated cloudy air can be either warmer or colder than the surrounding cloud. The warmest air in the dissipation track would be either adiabatically-heated cloud-free air pushed into the cloud from above without much mixing, or cloudy air that has been heated by latent heat released during ice formation, but not mixed with the aircraft downwash. However, if CTEI evaporation effects dominate, only unmixed dry downwash air would be warmer than the surrounding cloud.

Another fallout of this mechanism would be that the cloud effects induced by aircraft would be significantly influenced by the height at which the aircraft flies above cloud tops. At higher heights above cloud top, generally warmer and drier the air mixes into the cloud, and as shown in Fig. 7, the magnitude of the evaporation response should change.

Another prediction of this hypothesis would be that this mechanism should work even for clouds that are warmer than 0˚C and satisfy CTEI instability criterion. If a flight track is found at temperatures >0˚C, then obviously any mechanism involving freezing cannot explain the cloud dissipation. Therefore it would be prudent to observe stratiform cloud decks that are above freezing in regions of aircraft traffic for these “canal tracks” as aircraft fly over. Similarly, cirrus clouds composed entirely of ice particles would also be susceptible to CTEI, since clouds composed of frozen or liquid water have similar potential to evaporate when mixed with warmer air as aircraft fly above. However, as shown in Fig. 9b the intensity of any CTEI effects should diminish with decreasing temperature.

Both the CTEI mechanism and the seeding-induced cloud dissipation processes are turbulence-scale processes. Thus, relatively high vertical resolution (1-10s of meters) measurements would be required of the condensed water content, temperature and relative humidity across the cloud top layer and into the cloud-free area above a cloud in order to fully document the turbulent propagation effects associated with either evaporation or freezing. It would be valuable to measure turbulent properties within seeding/dissipation tracks, and additional measurements of microphysical phase using another aircraft flying through a seeded cloud would be extremely valuable, however, these measurement aircraft would be introducing another downwash turbulent artifact into the system.

6. Conclusions

Aircraft flying within and above clouds "vertically-stirs" or "seeds" clouds with turbulence, and this turbulent downwash can have a significant impact if the gradients of temperature, relative humidity and condensed water content satisfy well-established cloud top entrainment instability (CTEI) criterion. If CTEI criterion are satisfied near cloud top, then aircraft downwash can potentially trigger an unstable evaporation process which could propagate laterally to considerable horizontal distances away from a flight track, driven by the cooling associated with cloud evaporation and dissipation. There are many obvious and simple-to-perform experiments of this proposed hypothesis that warrant further investigation. While phase change and ice formation has been observed in some cloud seeding experiments, the effects associated with evaporation have been neglected in past explanations of cloud seeding. If this evaporation mechanism occurs as aircraft fly close to the tops of stratiform clouds, then current and past meteorology textbooks describing cloud seeding provide only a partial explanation of the physics and dynamics of the observed dissipation.

1 Acknowledgements. The author is grateful to Dr. Duncan Blanchard, who flew on many of the
2 original project CIRRUS seeding missions, and provided invaluable advice and commentary.
3 Also Geoffrey P. Williams, Archivist at the University at Albany Library Special Collections and
4 Archives, provided valuable assistance in browsing through mountains of archival notes and
5 reports from the Vincent Schaefer collection.

6 References

7 Aguado, E., Burt, J. E., 2009. Understanding weather and climate. Prentis Hall, New York.

8 Danielson, E. W., Levin, J., Abrams, E., 2003. Meteorology. McGraw-Hill, New York.

9 Greene, G. C., 1986. An approximate model of vortex decay in the atmosphere. J. Aircraft, 23,
10 566-573.

11 Heymsfield, A. J., Kennedy, P. C., Massie, S., Schmitt, C., Want S., Haimov, S., Rangno, A.,
12 2010. Aircraft-induced hole punch and canal clouds. Bull. Amer. Meteor. Soc. 91, 753-766.

13 Heymsfield, A. J., Thompson, G., Morrison, H., Bansemer, A., Rasmussen, R. M., Minnis, P.,
14 Wang Z., Zhang, D., 2011. Formation and spread of aircraft-induced holes in clouds. Nature 333,
15 77-81.

16 Langmuir, I., Forbes, A., 1936. Airplane tracks in the surface of stratus clouds. J. Aeronautical.
17 Sci. Soc., 3, 385–387.

18 Lilly, D. K., 1968. Models of cloud-topped mixed layers under a strong inversion. Quart. J. Roy.
19 Meteor. Soc., 94, 292–309.

1 Lutgens, F. K., Tarbuck, E. J., Tasa, D., 2006. The atmosphere: an introduction to meteorology,
2 10th edition. Prentis Hall, New York.

3 Mason, B. J., 1957. The physics of clouds. Oxford at the Clarendon Press, Oxford, UK.

4 Miller, A., Anthes, R. A., 1980. Meteorology, Charles E. Merrill Publishing Co., London.

5 Moran, J. M., 1994. Meteorology: the atmosphere and the science of weather. Macmillian
6 College Publishing Co. Inc., New York.

7 Rogers, R. R., Yau M. K., 1989. A short course in cloud physics, 3rd edition. Pergammon Press,
8 New York.

9 Rosenfeld, D., Xu, X., Dai, J., 2005. Satellite-retrieved microstructure of AgI seeding tracks in
10 supercooled layer clouds. J. Appl. Meteor., 44, 760-767.

11 Schaefer, V. J., 1946. The production of ice crystals in a cloud of supercooled water droplets.
12 Science, 104, 457-459.

13 Schaefer, V. J., 1949. The formation of ice crystals in the laboratory and the atmosphere. Chem.
14 Rev., 44, 291-320.

15 Schaefer, V. J., 1950a. The effects produced by seeding supercooled clouds with dry ice and
16 silver iodide. Centenary Proceedings of the Royal Meteorological Society, 42-50.

17 Schaefer, V. J., 1950b. Experimental meteorology. J. Appl. Math. Phys., 1, 153-236.

18 Wallace, J. M., and Hobbs, P. V., 1977. Atmospheric science an introductory survey. Academic
19 Press, New York.

1 Wallace, J. M., and Hobbs, P. V., 2006. Atmospheric science an introductory survey-2nd edition,
2 Elsevier Inc., New York.

3 Yamaguchi, T., Randall, D. A., 2008. Large-eddy simulation of evaporatively driven entrainment
4 in cloud-topped mixed layers. J. Atmos. Sci., 65, 1481-1504.

5 Yu, X., Rosenfeld, D., Lei, H., Xu, X., Fan, P., Chen, Z., 2005. Comparison of model-predicted
6 transport and diffusion of seeding material with NOAA satellite-observed seeding track in
7 supercooled layer clouds. J. Appl. Meteor., 44, 749-759.

8

Figure Captions

FIG. 1. "Racetrack" cloud dissipation pattern photographed 24 minutes after a B17 aircraft completed flying the pattern 100 meters above cloud top at 2070m ASL for 13 minutes at a speed of 76 m s^{-1}. The temperature at the top of this 700-m thick cloud was -5.6 ˚C, and the temperature lapse rate measured between the base and top of the cloud was -4 ˚C km^{-1}. The longer sides of the oval shape are about 29 km long, and the path cleared is 2-3 km wide. Crushed dry ice pellets with diameter 5-10 mm were dispensed through a small hole in the B17 floor at a rate of 480 g km^{-1}. Picture was taken at 11:21AM local time on 24 Nov 1948 over Utica NY. Note that dissipated cloud did not penetrate to cloud base.

FIG. 2. MODIS satellite image above the Texas-Arkansas-Louisiana border region showing numerous "flight tracks" cleared by aircraft in a stable stratiform cloud layer. Figure taken from Heymsfield et al., (2010). Here it is suggested that cloud dissipation of 2-3 km wide tracks results from evaporation of cloudwater (not freezing) via the propagation of a positive-feedback cloud top entrainment instability (CTEI) mechanism, triggered by the turbulent aircraft wake downwash produced while flying over the tops of these clouds pushing dry warm air into the cloud, triggering a feedback of entrainment, followed by evaporation producing negatively buoyant air generating more turbulent mixing.

FIG. 3. Downwash and vortex pair below a B-777-200 aircraft (estimated mass 1.45×10^5 kg) flying immediately above a 150 m thick cloud while approaching London Gatwick airport at 7AM local daylight time on 10 July 2006. Surface temperature was 16 ˚C. Aircraft was descending through an altitude of 0.61 km at a speed of about 108 m s^{-1}. Photograph courtesy of Steve Morris photographer, who was positioned about 9 km in front of the approaching aircraft at the surface, using a 840mm telephoto lens. Cloud in this viewing area was reported to

completely dissipate 20 minutes after the photograph was taken. It is suggested here that these aircraft-scale vortices can under many conditions laterally propagate via the release of cloud-top entrainment instability, dissipating by evaporation much larger cleared tracks shown in Figs. 1-2.

FIG. 4. Downward vertical displacement of aircraft wake vortex below aircraft before ultimate dissipation as a function of atmospheric static stability according to a generalized semi-empirical wake vortex model of Greene (1986). General scale on left is displacement normalized by aircraft wingspan. Scale on right is for the 32m wingspan of a B17 seeding aircraft. During project Cirrus, temperature lapse rates were only measured between the base and top of the seeded clouds and ranged from 6-8 ˚K km^{-1}, shown as a grey shaded area.

FIG. 5. Schematic of the temperature structure near the top of the Fig. 1 "racetrack" cloud. Adiabatically-heated air forced down by aircraft into the cloud mixes with cooler cloudy air. Under the right Rh/stability conditions, some mixtures can become colder than the cloud and freely descend further into the cloud, initiating a positive-feedback turbulence/evaporation cycle, releasing cloud top entrainment instability.

FIG. 6. Virtual temperature difference (solid lines) and liquid water content (dashed lines) of mixtures of air 0.4 ˚C warmer mixed with a cloud containing 0.2 g kg^{-1} water at -5.6 ˚C, 790 hPa (Fig. 1 cloud conditions). When parcels colder than the cloud are produced, the coldest mixtures occur at the mixing fraction where all condensed water evaporates and final mixture Rh is 100%.

FIG. 7. (a) Maximum temperature difference, and (b) percentage of mixtures that are negatively buoyant, of mixtures of cloud-free air mixed into a cloud as a function of temperature (horizontal axis) and the relative humidity (vertical axis) of dry air mixed into the cloud. Cloud contains 0.2 g kg^{-1} water at -5.6 ˚C, 790 hPa (Fig. 1 cloud conditions). Temperature difference (Fig. 7a) is

calculated at the mixing fraction where all liquid water evaporates during mixing (minimum negative temperature shown on Fig. 6). Grey areas are regimes where negative buoyancy (unstable conditions) occurs. "X" denotes the conditions of the three curves shown in Fig. 6.

FIG. 8. Schematic of the thermodynamics describing the initiation of seeding-induced turbulence near the top of a stable cloud. Air warmed by the release of latent heat from the conversion of water liquid and vapor to ice will buoyantly rise in a stable environment. Updrafts will turbulently mix seeded ice nuclei into neighboring cloudy regions propagating the freezing-updraft cycle.

FIG. 9. Warming or cooling induced by (a) condensation/freezing or (b) mixing-induced evaporation as a function of cloud-top temperature. Warming due to freezing assumes 0.2 g kg^{-1} liquid to ice, and vapor in excess of ice saturation for a supercooled cloud at three different pressure levels. Most warming produced by glaciating a supercooled cloud arises from vapor condensation onto ice. Maximum cooling due to evaporation of cloud liquid water is calculated assuming 65% Rh air that is 0.2 ˚C warmer is mixed with cloudy air. "x" markings note the conditions of the warmer "racetrack" cloud (Fig. 1) near -6˚C, 800mb, and colder "figure-4" cloud shown in Fig. 10 (-15˚C, 580mb).

FIG. 10. Virtual temperature difference of mixtures of air 0.4 ˚C warmer mixed with a cloud containing 0.2 g kg^{-1} water at -5.6 ˚C, 790 hPa. The original curve showing the greatest cooling (same as Fig. 6, 50% Rh) considers only evaporation and adjustment to liquid saturation. The line showing less cooling results from additional latent heating of supercooled cloud water converted to ice before mixing and evaporation to ice saturation.

FIG. 11. Portions of an 87 km-long "Figure-4" cloud dissipation pattern produced by dispensing seeding agents during CIRRUS project flight #83 on 18 Apr 1949, 10:06-10:20 am local time. Cloud top was -15°C, 4450 m (14600 ft) elevation. Cloud base was -7°C at 2591 m (8500 ft). Cloud thickness was 1860m, and the lapse rate within the cloud layer was -4.3 °C km^{-1}. Seeding aircraft dispensed dry ice along most of the pattern, but along the path at the right, the dry ice dispensing was interrupted for about three miles (one mile of nothing, followed by 1 mile of red-hot charcoal-impregnated with AgI, followed by another mile of no seeding). Approximate scale of the flight leg on the left is derived from project flight logs.

FIG. 12. Seeding aircraft dispensing dry ice photographed from an observing aircraft about 2 km above. Using the aircraft wingspan (32m), and the reported flight speed (99 m s^{-1}), the scale overlaid parallel to the emerging cloud channel shows the approximate time after (top) and distance behind (lower) the seeding flyover at the time of the photo. Cloud is visibly perturbed within ~4 seconds following seeding ~400 m aft of the aircraft flying <100m above cloud top. These times are too short for any appreciable freezing to occur, but are consistent with a downwash wake impacting the cloud top. Channel width grows from 54-99 m in ~13 seconds, a growth rate more than sufficient to produce 2-3 mile wide channel within 24 minutes if growth continues at this initial rate.

FIG. 1. "Racetrack" cloud dissipation pattern photographed 24 minutes after a B17 aircraft completed flying the pattern 100 meters above cloud top at 2070m ASL for 13 minutes at a speed of 76 m s^{-1}. The temperature at the top of this 700-m thick cloud was -5.6 ˚C, and the temperature lapse rate measured between the base and top of the cloud was -4 ˚C km^{-1}. The longer sides of the oval shape are about 29 km long, and the path cleared is 2-3 km wide. Crushed dry ice pellets with diameter 5-10 mm were dispensed through a small hole in the B17 floor at a rate of 480 g km^{-1}. Picture was taken at 11:21AM local time on 24 Nov 1948 over Utica NY. Note that dissipated cloud did not penetrate to cloud base.

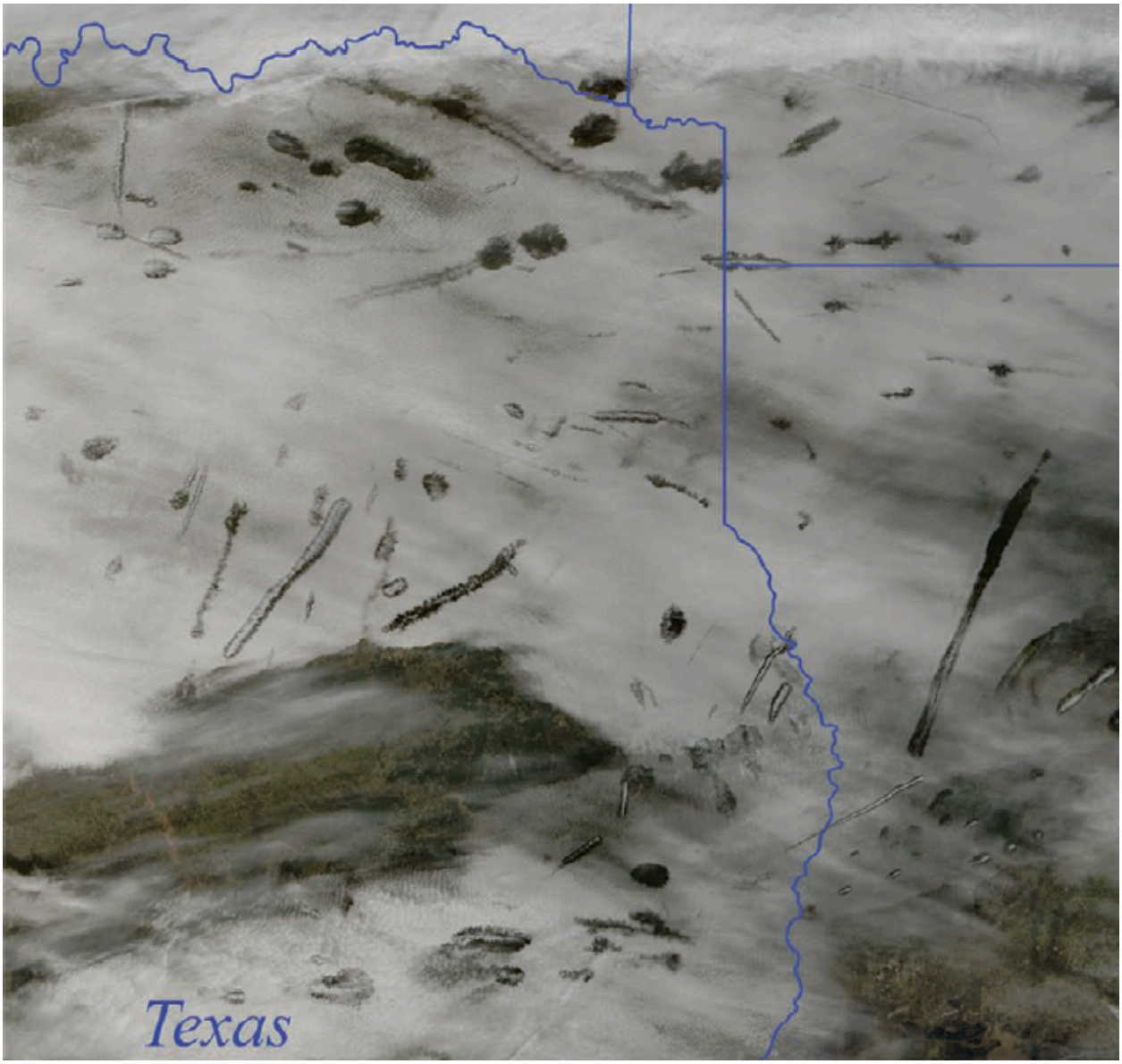

FIG. 2. MODIS satellite image above the Texas-Arkansas-Louisiana border region showing numerous "flight tracks" cleared by aircraft in a stable stratiform cloud layer. Figure taken from Heymsfield et al., (2010). Here it is suggested that cloud dissipation of 2-3 km wide tracks results from evaporation of cloudwater (not freezing) via the propagation of a positive-feedback cloud top entrainment instability (CTEI) mechanism, triggered by the turbulent aircraft wake downwash produced while flying over the tops of these clouds pushing dry warm air into the cloud, triggering a feedback of entrainment, followed by evaporation producing negatively buoyant air generating more turbulent mixing.

FIG. 3. Downwash and vortex pair below a B-777-200 aircraft (estimated mass 1.45×10^5 kg) flying immediately above a 150 m thick cloud while approaching London Gatwick airport at 7AM local daylight time on 10 July 2006. Surface temperature was 16 ˚C. Aircraft was descending through an altitude of 0.61 km at a speed of about 108 m s^{-1}. Photograph courtesy of Steve Morris photographer, who was positioned about 9 km in front of the approaching aircraft at the surface, using a 840mm telephoto lens. Cloud in this viewing area was reported to completely dissipate 20 minutes after the photograph was taken. It is suggested here that these aircraft-scale vortices can under many conditions laterally propagate via the release of cloud-top entrainment instability, dissipating by evaporation much larger cleared tracks shown in Figs. 1-2.

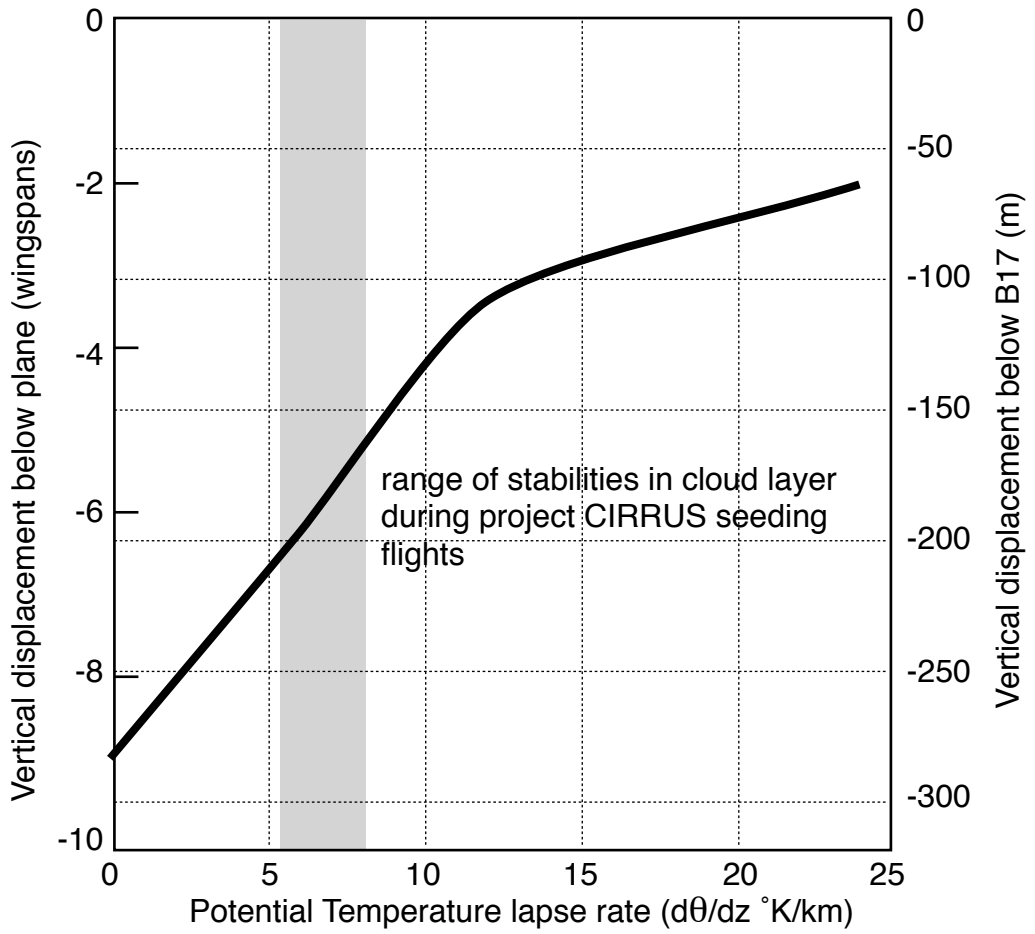

FIG. 4. Downward vertical displacement of aircraft wake vortex below aircraft before ultimate dissipation as a function of atmospheric static stability according to a generalized semi-empirical wake vortex model of Greene (1986). General scale on left is displacement normalized by aircraft wingspan. Scale on right is for the 32m wingspan of a B17 aircraft. Typical temperature lapse rates at tropospheric cloud layers of 6-8 ˚K km^{-1} are shown as a grey shaded range.

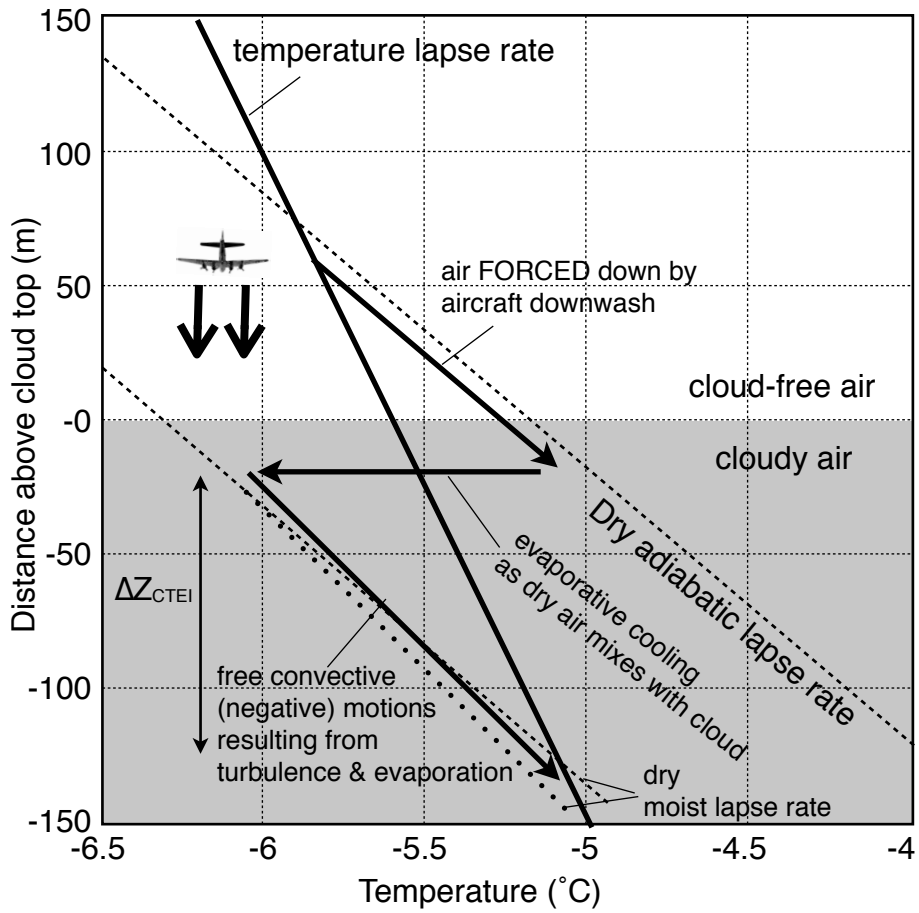

FIG. 5. Schematic of the temperature structure near the top of the Fig. 1 "racetrack" cloud. Adiabatically-heated air forced down by aircraft into the cloud mixes with cooler cloudy air. Under the right Rh/stability conditions, some mixtures can become colder than the cloud and freely descend further into the cloud, initiating a positive-feedback turbulence/evaporation cycle, releasing cloud top entrainment instability.

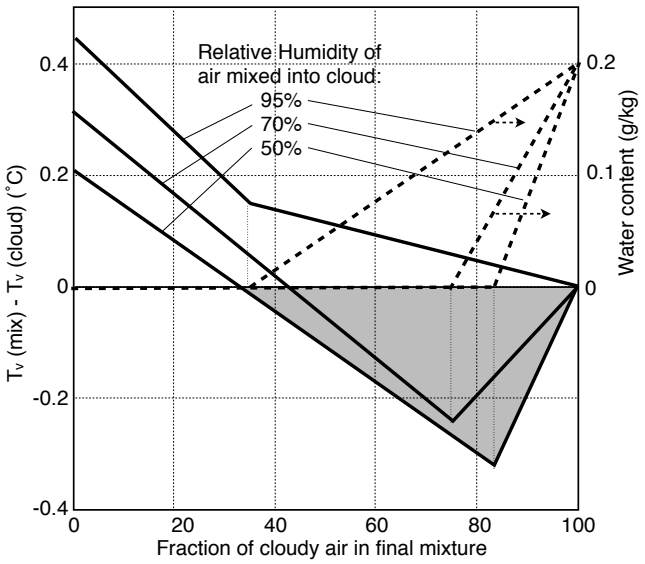

FIG. 6. Virtual temperature difference (solid lines) and liquid water content (dashed lines) of mixtures of air 0.4 ˚C warmer mixed with a cloud containing 0.2 g kg^{-1} water at -5.6 ˚C, 790 hPa (Fig. 1 cloud conditions). When parcels colder than the cloud are produced, the coldest mixtures occur at the mixing fraction where all condensed water evaporates and final mixture Rh is 100%.

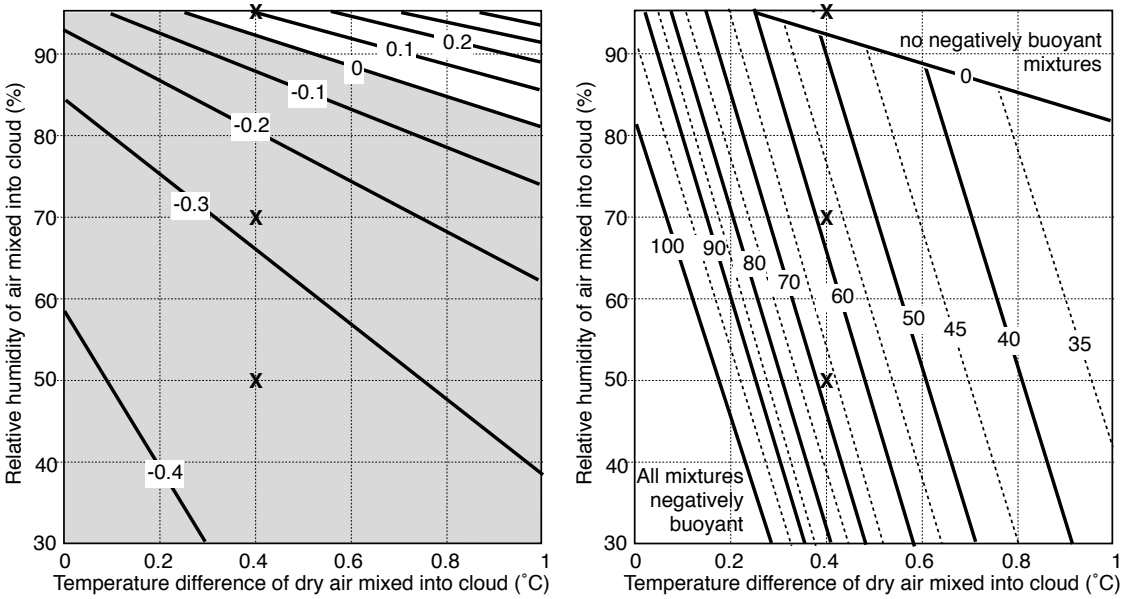

FIG. 7. (a) Maximum temperature difference, and (b) percentage of mixtures that are negatively buoyant, of mixtures of cloud-free air mixed into a cloud as a function of temperature (horizontal axis) and the relative humidity (vertical axis) of dry air mixed into the cloud. Cloud contains 0.2 g kg^{-1} water at -5.6 ˚C, 790 hPa (Fig. 1 cloud conditions). Temperature difference (Fig. 7a) is calculated at the mixing fraction where all liquid water evaporates during mixing (minimum negative temperature shown on Fig. 6). Grey areas are regimes where negative buoyancy (unstable conditions) occurs. "X" denotes the conditions of the three curves shown in Fig. 6.

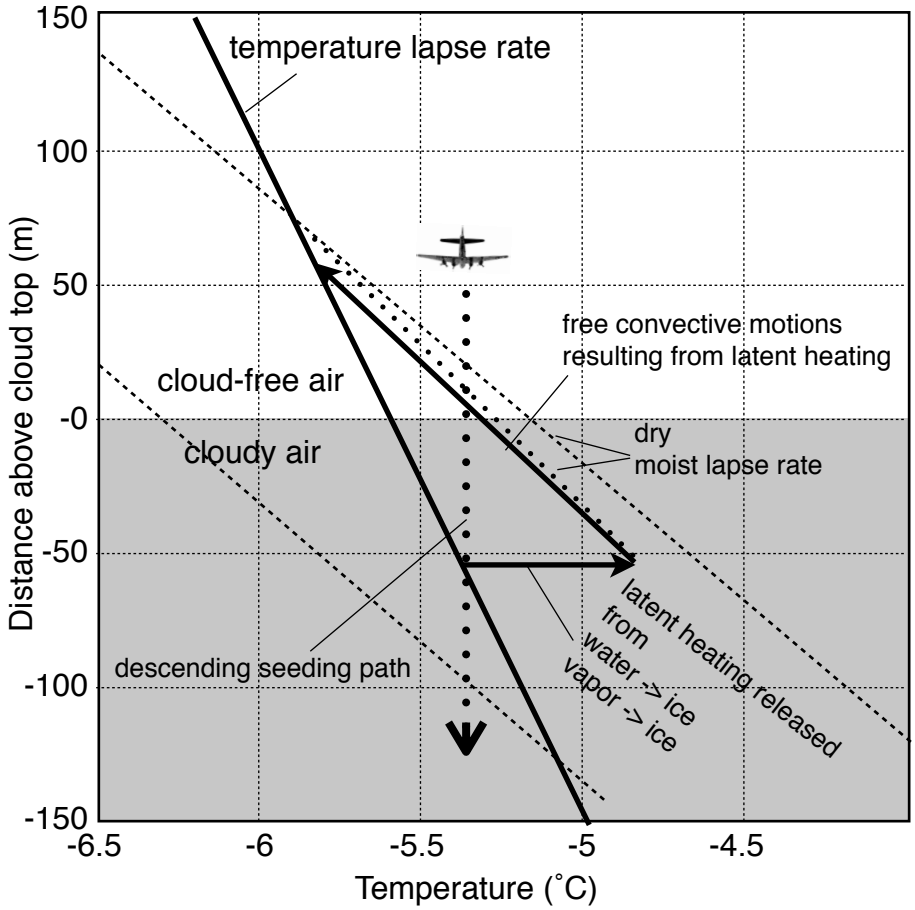

FIG. 8. Schematic of the thermodynamics describing the initiation of seeding-induced turbulence near the top of a stable cloud. Air warmed by the release of latent heat from the conversion of water liquid and vapor to ice will buoyantly rise in a stable environment. Updrafts will turbulently mix seeded ice nuclei into neighboring cloudy regions propagating the freezing-updraft cycle.

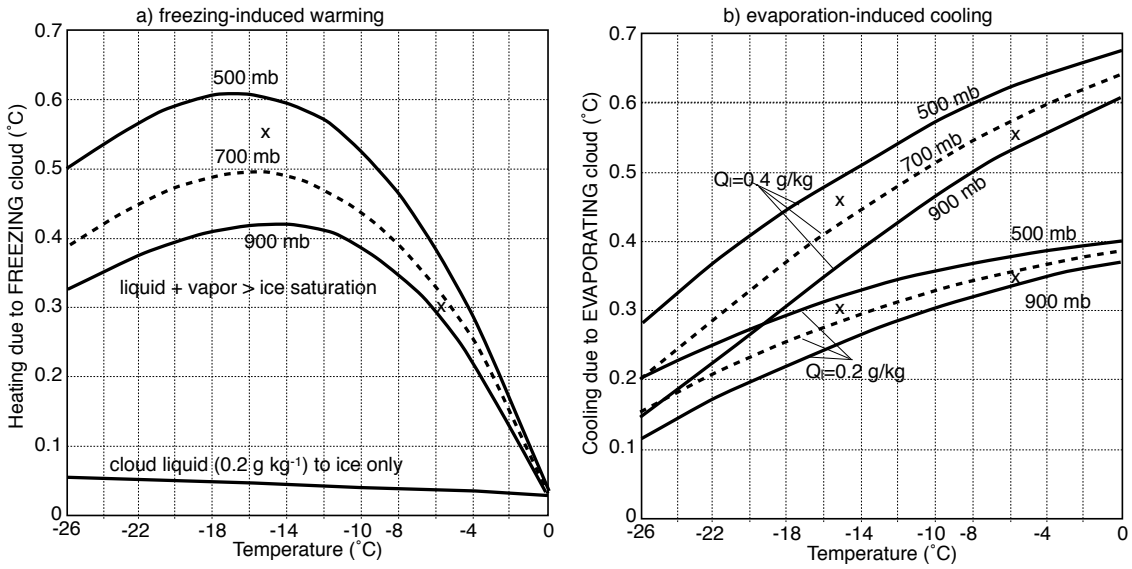

FIG. 9. Warming or cooling induced by (a) condensation/freezing or (b) mixing-induced evaporation as a function of cloud-top temperature. Warming due to freezing assumes 0.2 g kg^{-1} liquid to ice, and vapor in excess of ice saturation for a supercooled cloud at three different pressure levels. Most warming produced by glaciating a supercooled cloud arises from vapor condensation onto ice. Maximum cooling due to evaporation of cloud liquid water is calculated assuming 65% Rh air that is 0.2 ˚C warmer is mixed with cloudy air. "x" markings note the conditions of the warmer "racetrack" cloud (Fig. 1) near -6˚C, 800mb, and colder "figure-4" cloud shown in Fig. 10 (-15˚C, 580mb).

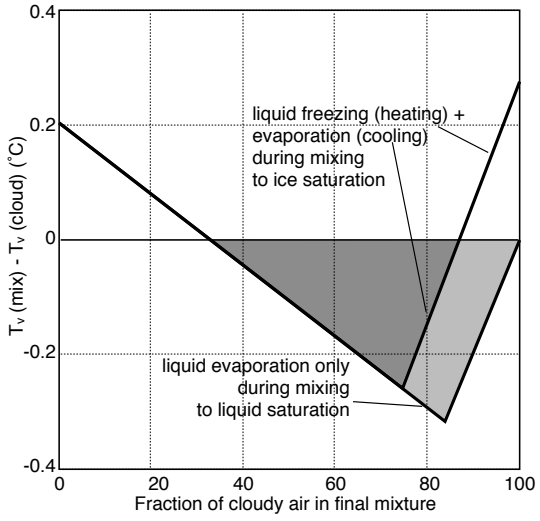

FIG. 10. Virtual temperature difference of mixtures of air 0.4 ˚C warmer mixed with a cloud containing 0.2 g kg^{-1} water at -5.6 ˚C, 790 hPa. The original curve showing the greatest cooling (same as Fig. 6, 50% Rh) considers only evaporation and adjustment to liquid saturation. The line showing less cooling results from additional latent heating of supercooled cloud water converted to ice before mixing and evaporation to ice saturation.

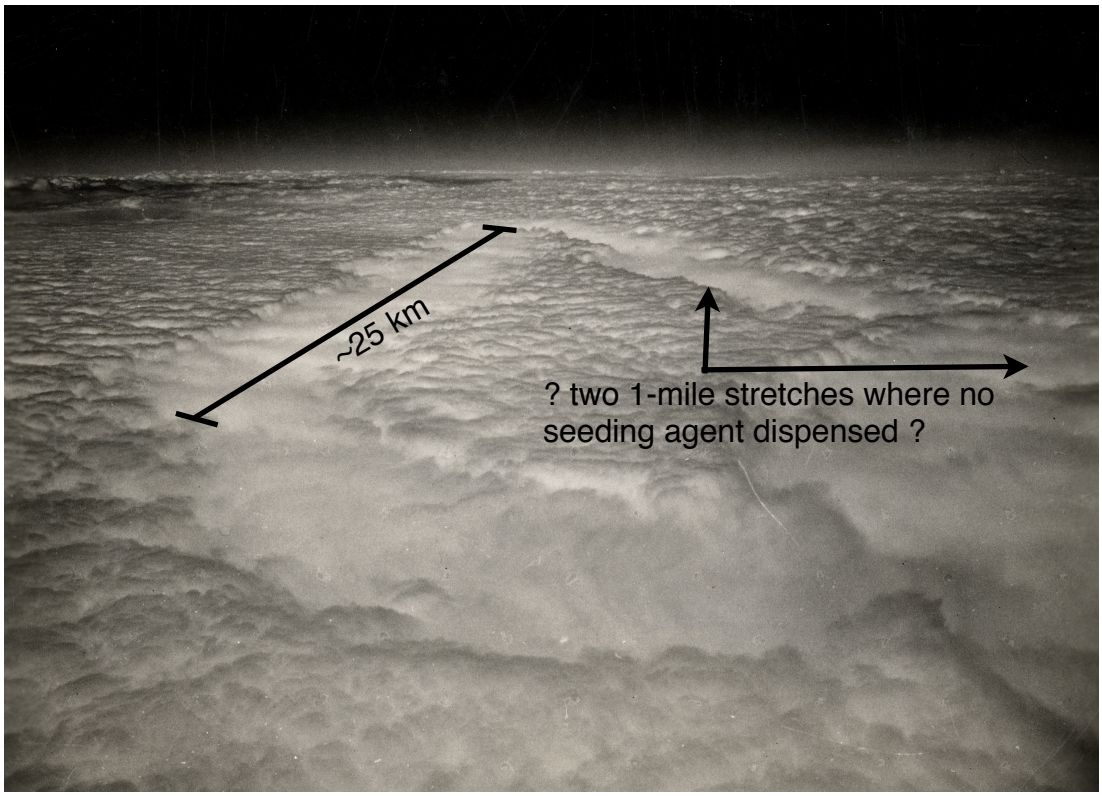

FIG. 11. Portions of an 87 km-long "Figure-4" cloud dissipation pattern produced by dispensing seeding agents during CIRRUS project flight #83 on 18 Apr 1949, 10:06-10:20 am local time. Cloud top was -15°C, 4450 m (14600 ft) elevation. Cloud base was -7°C at 2591 m (8500 ft). Cloud thickness was 1860m, and the lapse rate within the cloud layer was -4.3 °C km^{-1}. Seeding aircraft dispensed dry ice along most of the pattern, but along the path at the right, the dry ice dispensing was interrupted for about three miles (one mile of nothing, followed by 1 mile of red-hot charcoal-impregnated with AgI, followed by another mile of no seeding). Approximate scale of the flight leg on the left is derived from project flight logs.

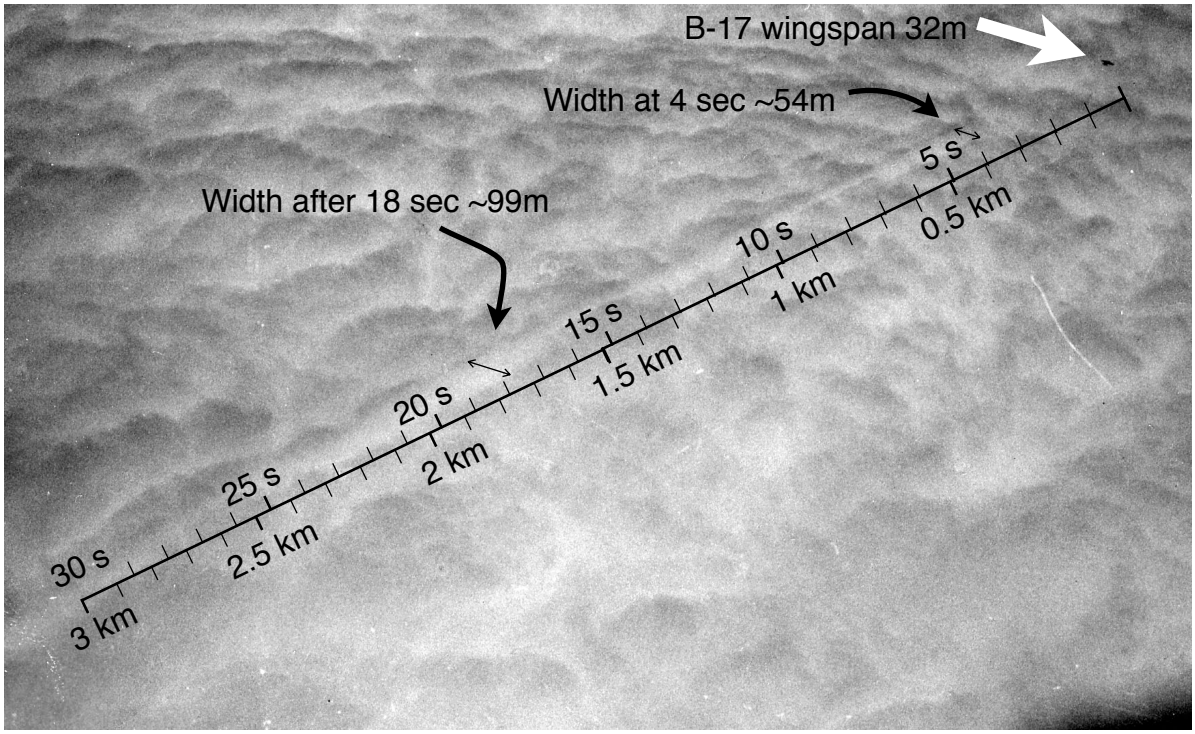

FIG. 12. Seeding aircraft dispensing dry ice photographed from an observing aircraft about 2 km above. Using the aircraft wingspan (32m), and the reported flight speed (99 m s^{-1}), the scale overlaid parallel to the emerging cloud channel shows the approximate time after (top) and distance behind (lower) the seeding flyover at the time of the photo. Cloud is visibly perturbed within ~4 seconds following seeding ~400 m aft of the aircraft flying <100m above cloud top. These times are too short for any appreciable freezing to occur, but are consistent with a downwash wake impacting the cloud top. Channel width grows from 54-99 m in ~13 seconds, a growth rate more than sufficient to produce 2-3 mile wide channel within 24 minutes if growth continues at this initial rate.